How did Early Stages of the Universe Shape Its Evolution into its Current State?

Bo-Jun Qin

Received October 21, 2023
Accepted March 06, 2024
Electronic access March 15, 2024

The early universe holds vital information regarding the nature of the universe. The cosmic microwave background (CMB), containing remaining radiation from the first light in the universe, is currently the only object that can provide evidence for inflation. In this paper, I simulate CMB signals from a power spectrum and analyze the effects of noise on the precise measurement of the CMB. The resulting power spectrum of the simulated CMB signal reveals to be biased high at smaller angular scales compared to the accepted power spectrum from the Planck satellite. I also simulate a 21-cm line signal from the epoch of reionization (EoR), the period when the first stars and galaxies formed, which has yet to be detected. Simulating signals from the early universe, while they may not completely accurately represent observed signals, offers valuable insight, predicting how undetected signals from inflation and the EoR may appear and assessing the possible noise factors that may affect those signals.

Introduction

The Big Bang theory hypothesizes that the universe began as a hot, tiny, compact ball of infinite density that expanded, rapidly at first and then slower afterwards, arriving at the current state that we know today. The Big Bang model assumes the existence of two early stages in the universe: inflation and the cosmic dark ages, both of which have yet to be detected. Inflation occurred right after the birth of the universe [1]. The cosmic dark ages mark the period of darkness in the universe between the formation of the cosmic microwave background and the epoch of reionization.

This paper aims to explain what inflation is and how it can be detected through the cosmic microwave background. This paper will also highlight the importance of advancements in the field of mm-wave astronomy and radio astronomy in order to observe inflation and the epoch of reionization, respectively. Ground-based telescopes observing the early universe currently face excess noise from astrophysical, environmental, and instrumental sources, some known, others unknown, all of which distort or mask the detection of signals. I simulate signals from the cosmic microwave background and epoch of reionization to analyze, compile, and communicate the effects of noise on observing those early stages of the universe. Reducing noise in ground-based telescopes, especially large, pioneering experiments containing thousands of detectors, begins with understanding the noise that affects them to reach the ultimate goal of revealing the nature and origin of the universe.

Inflation

Inflationary theory, proposed by physicist Alan Guth in 1979, states that the universe originated from the same patch of space, and from 10^{-36} seconds to between 10^{-33} and 10^{-32} seconds after the Big Bang, it underwent a rapid, exponential expansion. During this fraction of a second, the universe expanded by at least a factor of 10^{26}, causing the energy density of inhomogeneities, curvature, and both exotic and standard-model particles to fall [2]. As a result, the universe became relatively uniform and flat. Thus, the inflationary model resolves three inconsistencies in Big Bang cosmology: the magnetic monopole problem, the flatness problem, and the horizon problem.

Magnetic-monopole Problem

When Guth first proposed the inflationary theory, he was trying to solve the magnetic-monopole problem. The Grand Unified Theory, which suggests that three of the four fundamental forces—electromagnetic, strong, and weak—used to be one singular force before splitting up, predicts that the hot, early universe would produce a large amount of heavy, stable particles called magnetic monopoles [3]. However, they have yet to be observed in the universe today. Inflation, assuming that it happened at temperatures lower than that at which magnetic monopoles can be produced, explains this problem because its occurrence would dilute the density of magnetic monopoles exponentially so that they would be nearly undetectable.

Flatness Problem

The universe is observed to be nearly flat, having close to zero curvature, as its total energy density is similar to critical density[4]. If its density were greater than critical density, then its curvature would be positive; if less, then negative. However, any small amount of curvature that the universe had at its origin should grow with time and be noticeable today, yet it still appears nearly flat[5]. Inflation reconciles this problem: the exponential expansion of space in the early universe extensively smoothed out any initial curvature, making the universe seem flat today.

Horizon Problem

The horizon problem questions why the universe appears statistically homogeneous and isotropic. In the Standard Model of the Big Bang without inflation, two distant regions of space could not have interacted with one another when the universe just formed, because they moved apart faster than the speed of light. However, because inflation assumes that all regions of the universe began as one small patch of space, the universe can have one constant temperature and curvature.

Recent advancements in inflationary theory include the development of the first quantum field model of inflation[6] along with string-motivated models of inflation[7]. In order to provide concrete answers to these three problems, a measurement of inflation, specifically the tensor-to-scalar ratio r, also known as the energy scale of the universe, must be made to support inflation's occurrence. Currently, the cosmic microwave background is the only object that can provide this direct evidence through inflationary gravitational waves thought to be imprinted in the CMB polarization.

Cosmic Microwave Background

The cosmic microwave background (CMB) is a uniform microwave radiation, not associated with any astronomical object, that fills all space in the observable universe[8]. The CMB is the oldest observable light from the early universe, formed when the universe was approximately 380,000 years old[9]. Before then, the young universe was hot, dense, and opaque such that only baryons, electrons, and photons existed; atoms could not form. Photons, when emitted, could not release light because they would encounter an unbound electron and scatter. As the universe continued to expand, its temperature dropped to about 3000 Kelvin. Then, electrically neutral hydrogen atoms formed through the recombination of protons and electrons. Photons were released through decoupling: with fewer unbound electrons in the universe, they experienced less scattering when emitted and traveled freely through the universe, generating the first source of light[10]. The CMB captures the remnants of the radiation from the surface of last scattering that has since been redshifted due to the expansion of the universe and is now observed in the microwave range. These early photons cannot interact with today's matter, so they stay in the background of the universe.

The CMB was discovered in 1964 by Arnold Penzias and Robert Wilson. They were using a radio telescope to measure a supernova remnant in the constellation of Cassiopeia when they detected an unexpected, constant hiss despite pointing the telescope into empty space[11]. This turned out to be the CMB signal. Since its initial discovery, the temperature of the CMB has been measured to high precision at 2.72548 ± 0.00057 K[12]. Furthermore, the CMB behaves like a perfect blackbody, meaning that it is a perfect emitter and absorber[13].

Anisotropies

Although the CMB is overall uniform and homogeneous, tiny fluctuations called anisotropies exist and contain valuable information regarding the early universe. These anisotropies are divided into two types: primary and secondary. Primary anisotropies were imprinted into the CMB within those 380,000 years of the early universe before and during recombination[14]. Secondary anisotropies emerged after the CMB formed due to CMB photons interacting with electrons traveling at the speed of light in intergalactic gas as they traverse through over 14 billion years of space[15].

Temperature

The CMB temperature angular power spectrum displays CMB temperature anisotropies as a plot as shown in Figure 1. The x-axis measures the various angular scales, i.e. the relative angle between the observer and two points in the sky, at which the CMB is measured. As the angular scale decreases, the precision at which the CMB temperature anisotropies are measured increases. The multipole moment, l, equals 180 degrees divided by the angular scale. The y-axis measures the contribution of temperature fluctuations on a given angular scale compared to the overall variance of the fluctuations[16].

The peaks in the spectrum provide information about the nature of the universe. The location of the first and largest peak on the x-axis represents that the universe is flat, or nearly so, with $\pm 0.2\%$ curvature. The second and third peaks present the densities of ordinary and dark matter in the Universe, respectively, and they are surprisingly close to each other[17].

On the CMB map, temperature anisotropies show up as blue (cold) and red (hot) patches. The blue patches represent overdensities in structure, i.e. the presence of galaxy clusters, as those photons spent more energy escaping the gravitational pull from structure formation. Meanwhile, the red patches represent underdensities in structure, i.e. few to no galaxy clusters, as those CMB photons traveled freely through that space without a

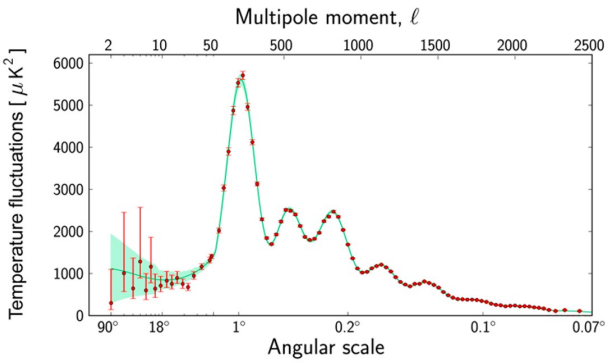

Fig. 1 The CMB power spectrum. Image from ESA and the Planck Collaboration [16]

significant decrease in energy [14].

Polarization

There are two types of polarization anisotropies in the CMB: E modes and B modes. E modes result from density perturbations, which relate to structure formation in the universe. They also correlate to CMB temperature: where there is a peak in the temperature power spectrum, there is a trough in the E mode power spectrum. B modes, on the other hand, result from gravitational waves from inflation, which polarize photons differently than structure formation does to produce E modes, and thus would provide evidence for the inflationary theory [18]. Figure 2 shows the difference between E and B modes.

B modes have been detected from gravitational lensing, but not from inflation, because as E-mode photons travel through fourteen billion years of space, some transform into B modes. Fortunately, the power spectrum of B modes from gravitational lensing looks different from what a B-mode power spectrum from inflation would look like. However, B modes from lensing overpower B modes from inflation, as seen in the B mode power spectrum, further complicating efforts to detect inflationary B modes [19].

Detecting B modes from gravitational waves is vital in determining r, the tensor-to-scalar ratio. Finding r provides the energy scale of inflation, i.e. the energy level of the universe required for inflation to occur, which is important in predicting the fate of the universe [19].

However, as noise, both from gravitational lensing and possible unknown sources, mask inflationary B modes, simulating CMB polarization signals can predict their appearance with noise and the possible causes of noise and verify future filtered observed signals with simulated ones without noise.

In the following section, I simulate a complete and realistic CMB temperature anisotropy signal while analyzing the effects of instrumental and environmental noise on the measurement of the signal. Then, I also apply those noises to simulated CMB polarization signals. Finally, I compare the power spectrum of the simulated CMB temperature anisotropy signal to that of signals observed by the Atacama Cosmology Telescope and the Planck satellite, which is presented in Figure 1.

The added noise in the simulated CMB temperature anisotropy signals replicates those disturbing the observations of large, pioneering experiments with telescopes of thousands of detectors. Simulating and understanding noise improves the calibration of telescopes and, in turn, measurements of inflation and other stages of the early universe.

Simulating CMB Signals

In this section, I simulate maps of the CMB and analyze the distorting effects of different types of noise. To simulate a CMB signal, I first read in a power spectrum generated by the Code for Anisotropies in the Microwave Background (CAMB), similar to Figure 1. Because I only consider a small, ten-by-ten-degree square patch of the CMB, I use a flat-sky approximation on the CAMB power spectrum and generate a 2D power spectrum by substituting a variable k for l, where $l = 2\pi k$. Then, I generate a Gaussian random map with unit variance, multiply that with the 2D power spectrum, and Fourier transform the result to produce a real space map [20].

A CMB temperature anisotropy map generated from telescopes include astrophysical features that distort the raw signal. In Figure 4, I simulate a CMB signal with foregrounds, i.e. point sources and the Sunyaev-Zel'dovich (SZ) effect. Point sources result from astronomical objects including active galactic nuclei and dust forming galaxies; they appear as small red specks on the CMB map [21]. The SZ effect occurs when a CMB photon receives an energy boost from a relativistic electron in a galaxy cluster and appears as small blue specks on the CMB map [15].

In addition to foregrounds of the universe, the CMB signal detected by telescopes suffers from noise, from both the instruments and the atmosphere. To make the simulated CMB temperature anisotropy map realistic to raw signals measured by telescopes, I add four different types of noise to the map and analyze their individual effects.

First, I convolve the map with a Gaussian beam pattern to mimic the diffraction from telescopes. Figure 5 shows the CMB signal convolved at three different beam sizes. As shown in the three different maps, increasing the beam size decreases the visibility of the point sources and SZ effects, blurs anisotropies in the red and blue patches, and highlights the white outline of red patches. This effect is most prominent in Figure 2c in which the beam size is 10.

Then, I generate a noise map and overlay it onto the convolved CMB map. The noise map consists of white noise (i.e. static), atmospheric noise (water vapor), and $1/f$ noise (from telescope detectors) [18]. In the following figures, I apply each type of noise

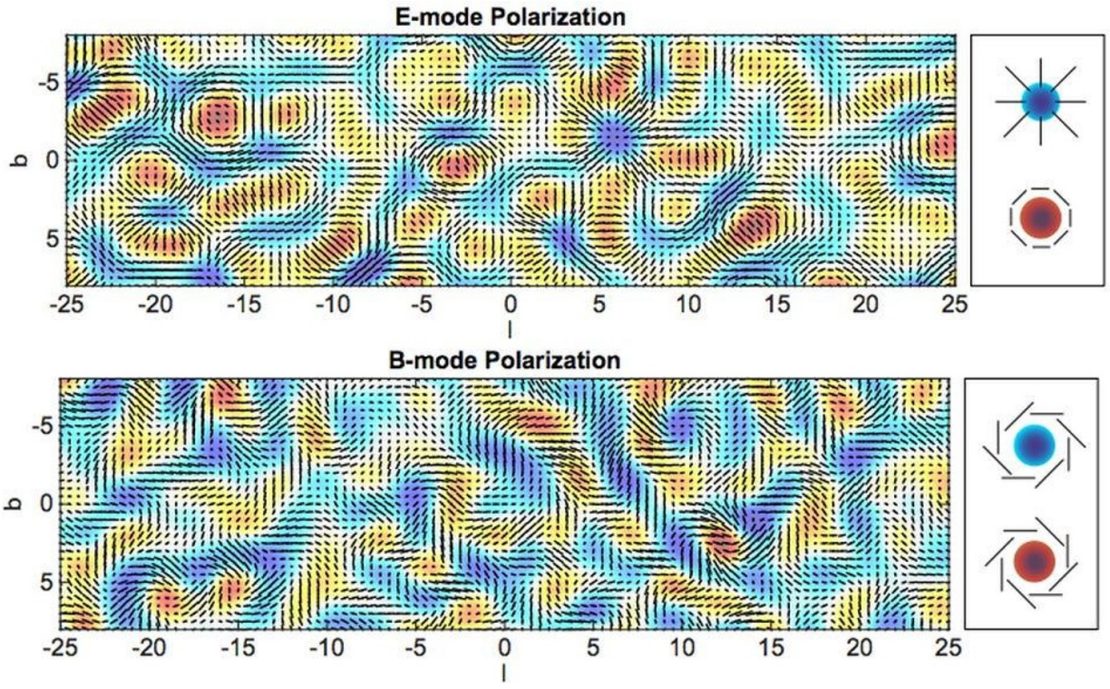

Fig. 2 Depiction of E-mode (top) and B-mode (bottom) polarization in the CMB [19].

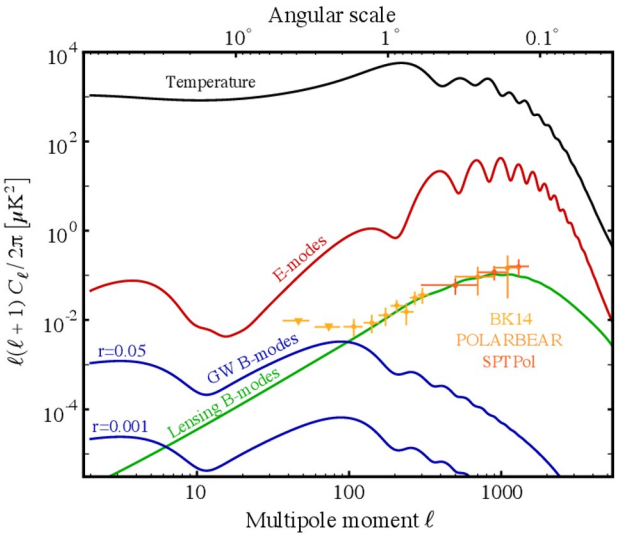

Fig. 3 The theoretical power spectra for the temperature (black), E modes (red), lensing B modes (green), and gravitational wave B modes (blue) [18].

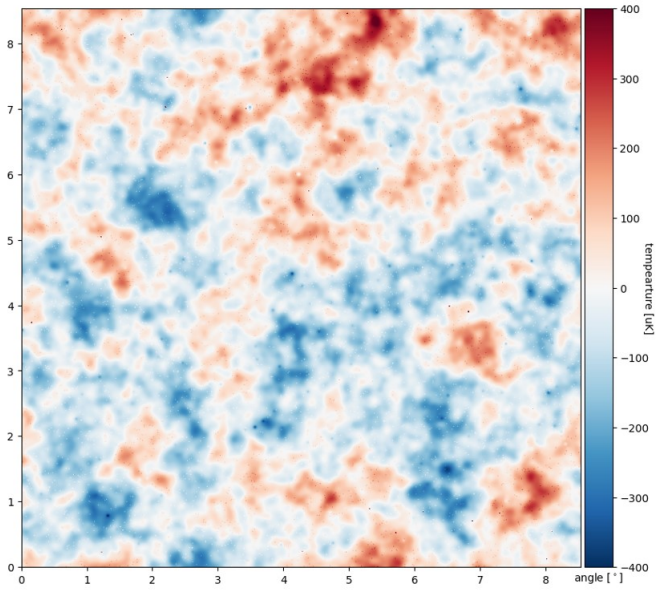

Fig. 4 Simulated CMB signal with points sources and SZ effect.

individually to the CMB map and at different values to examine their unique effects.

In Figure 6, I add three different levels of white noise to the CMB signal. White noise adds static—a spottiness—to the signal. As the white noise level increases, the map appears less smooth and more grainy. In Figure 6c, the signal overall appears darker, and the white patches outlining the red and blue patches that are present in Figures 6a and 6b disappear.

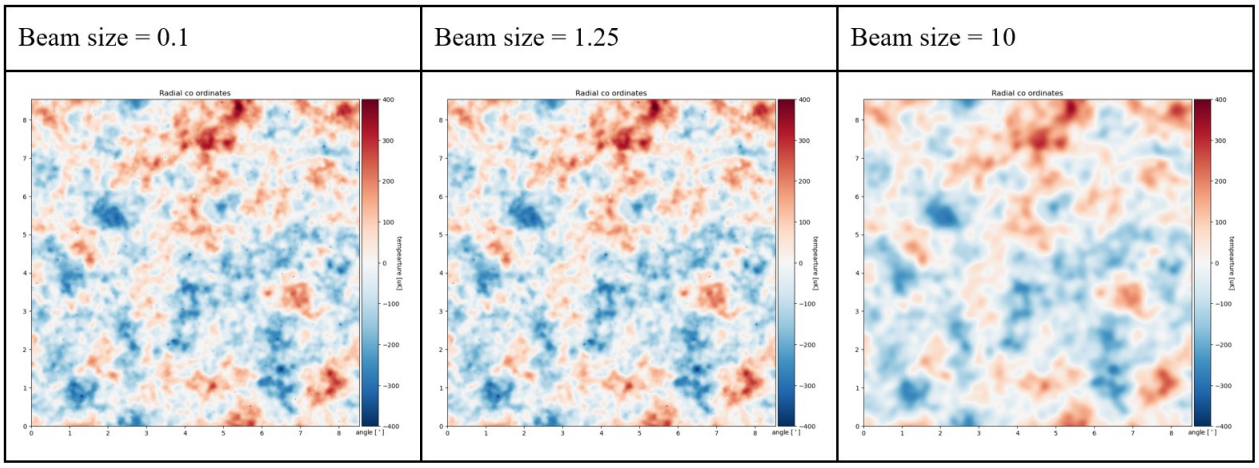

Fig. 5 (a), (b), (c): Simulated CMB temperature anisotropy map with foreground, i.e. from Figure 4, convolved with beam size of (a) 0.1, (b) 1.25, and (c) 10.

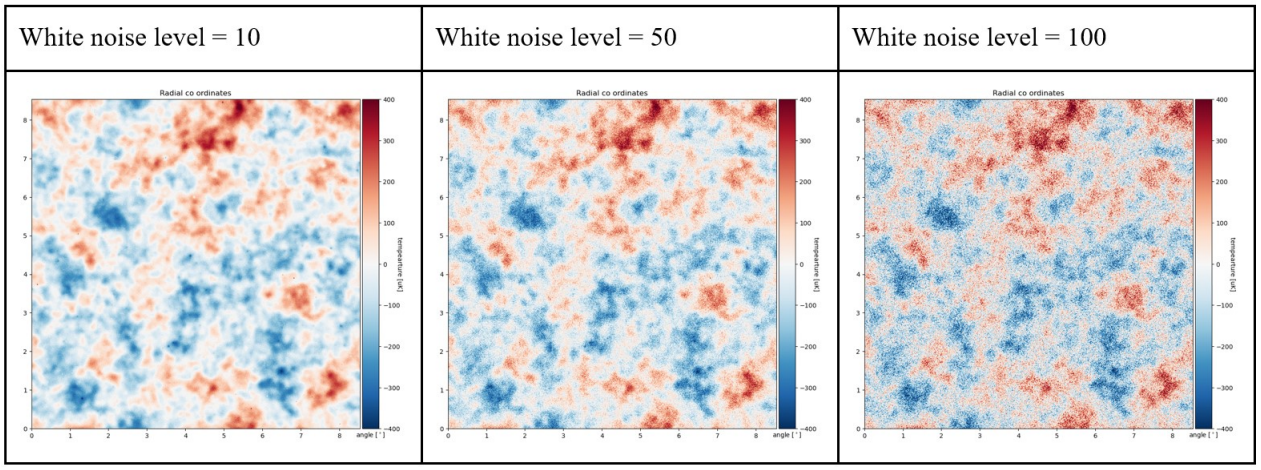

Fig. 6 (a), (b), (c): Convolved CMB temperature anisotropy map, i.e. Figure 5b, with white noise levels of (a) 10, (b) 50, and (c) 100. No other types of noise are present in these maps.

In Figure 7, I add three different levels of atmospheric noise to the CMB signal. As the level of atmospheric noise increases, more and darker red and blue patches not present in the original CMB signal appear on the map. For example, from Figure 7a to 7b, the red patch at the top of the map grew and became darker. The effect of atmospheric noise is best seen in the right half of Figure 7c where large, dark red patches, not present in the original map nor the maps of lower atmospheric noise level, appear and mask the actual CMB signal.

In Figure 8, I add three different levels of $1/f$ noise to the CMB signal. $1/f$ noise adds a stripiness to the map. At low $1/f$ noise levels as in Figure 8a, thin, horizontal, white lines appear across the map. At higher $1/f$ noise levels as in Figures 8b and 8c, the lines become more apparent and streakier and shift the locations of the patches.

I apply the beam convolution and all three types of noises to Figure 1, the CMB signal with point sources and SZ effect. I first convolve the signal at one beam size. Then, I choose one value for each type of noise and create a noise map. I overlay the noise map onto the convolved CMB signal, producing a realistic, raw CMB map as detected by telescopes in Figure 9.

I generate CMB polarization maps in a similar manner, first with points sources and SZ effect, then convolved, and finally overlaid with a noise map. As seen in figures 10 and 11, the foregrounds and noise distort the polarization maps more than they did the temperature map.

To compare the simulated CMB signal to an actual CMB signal, I use public data from a 148 GHz detector in the Atacama

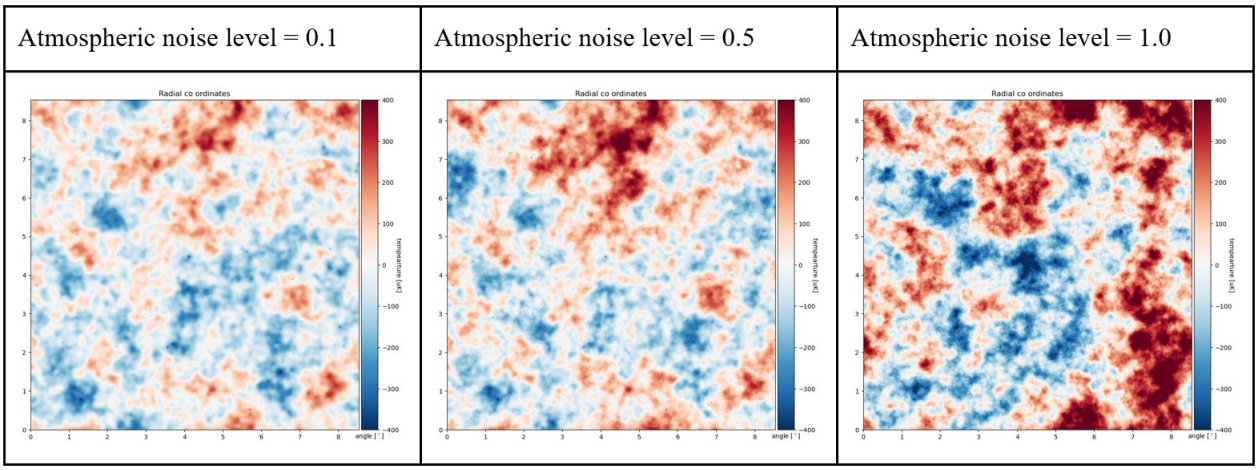

Fig. 7 (a), (b), (c): Convolved CMB temperature anisotropy map, i.e. Figure 5b, with atmospheric noise levels of (a) 0.1, (b) 0.5, and (c) 1.0. No other types of noise are present in these maps.

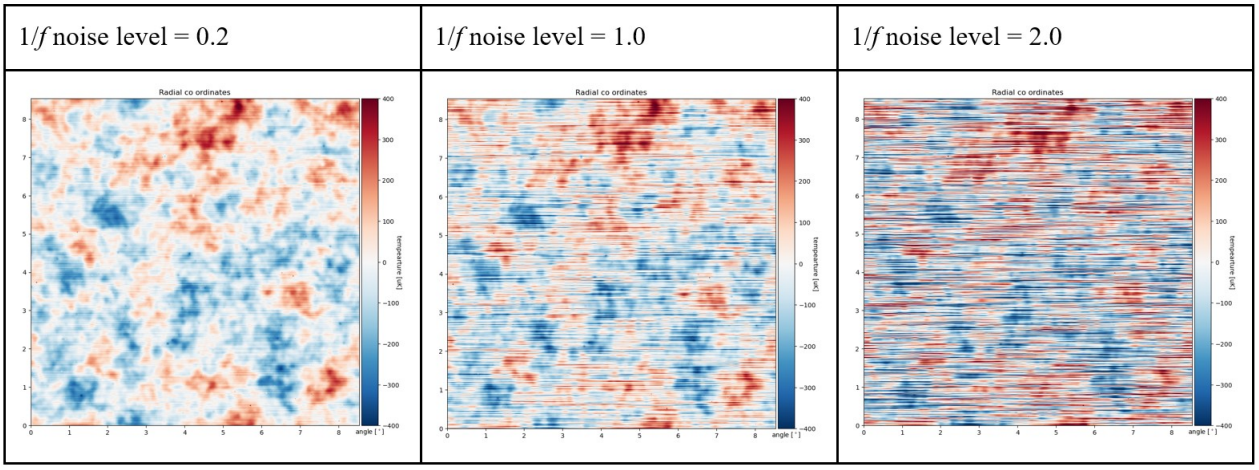

Fig. 8 (a), (b), (c): Convolved CMB temperature anisotropy map, i.e. Figure 5b, with $1/f$ noise levels of (a) 0.2, (b) 1.0, and (c) 2.0. No other types of noise are present in these maps.

Cosmology Telescope (ACT)[22]. Because the ACT map comes in long stripes, I cut a square patch of the data and do so for a similar size patch of the simulated signal. Then, I plot the power spectra of the ACT data and simulated (theory) data in Figure 12. Additionally, the green curve represents the actual, accepted CMB power spectrum observed by the Planck telescope.

The power spectrum of the simulated signal accurately represents those of the ACT signal and Planck signal on relatively small l (larger angular scales) from approximately $l = 500$ to $l = 2300$. However, the simulated signal deviates from the ACT signal on larger l as the ACT signal has higher power than the simulated signal does. This discrepancy could be attributed to the simulated signal representing a signal observed from a 150 GHz detector rather than a 148 GHz one. While this slight difference in frequency seems negligible, it is possible that a signal observed by a detector of one frequency could have more power than that from the other, yet as Figure 12 suggests, the power spectrum of the simulated signal should be higher than that of the ACT signal, because higher frequency detectors are more sensitive than lower frequency ones. Albeit the difference in frequency is relatively miniscule, the power spectrum of the simulated signal is not higher than that of the ACT signal and is in fact lower on larger l. Another possible source of error is that real, observed SZ effects have clusters of various sizes; however, those in the simulated signal have clusters of only one size which may affect the resulting power spectrum. Furthermore, the simulated noise may not fully represent the effects of actual noise, hence causing the power spectrum of the simulated signal

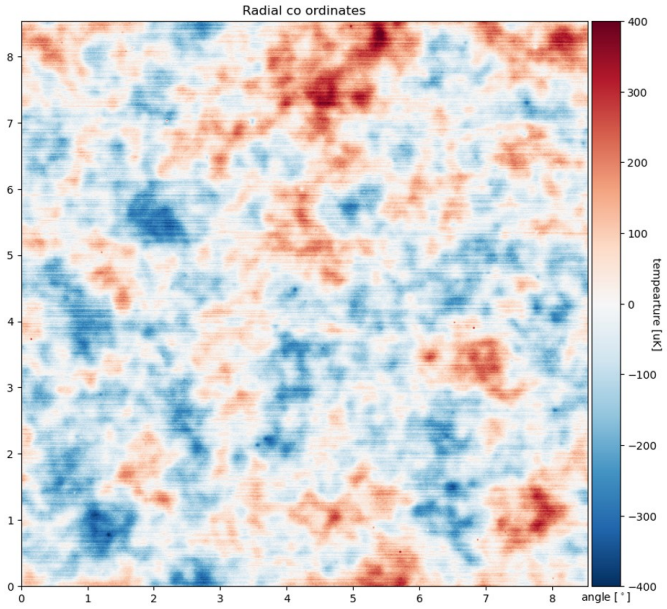

Fig. 9 Simulated CMB temperature anisotropy map convolved with beam size 1.25. The noise levels for white noise, atmospheric noise, and $1/f$ noise are, respectively, 10, 0.1, and 0.2.

to deviate from that of the ACT signal on larger l. Additionally, both the simulated and ACT signals bias high compared to the Planck signal starting from around $l = 2000$.

I also generate the power spectra of data from a 148 GHz and a 220 GHz detector in the ACT as shown in Figure 13. The power spectrum of the 220 GHz detector is biased high for all l compared to that of the 148 GHz detector, indicating that higher-frequency telescopes are more sensitive to atmospheric noise than lower-frequency ones are.

To summarize, this section analyzed how four different types of noise impacts the CMB temperature anisotropy signal observationally. Beam convolution decreases the visibility of points sources and SZ effect, blurs anisotropies, and highlights white outlines around the red patches. White noise adds grain to the signal and darkens anisotropies. Atmospheric noise adds red and blue patches not present in the original signal. $1/f$ noise creates thin stripes in the signal and shifts the positions of anisotropies.

I also compared the power spectra of the simulated, observed ACT, and Planck satellite CMB signals. Both the power spectra of the simulated and observed ACT signals are biased high on larger l compared to the accepted power spectrum of Planck signal, implying that the noise faced by ground-based telescopes hinders the detection of CMB temperature anisotropies at increased precision. Atmospheric noise seems to contribute to this disparity, as it is present on Earth but not in space and adds strength to the CMB signal, which explains why the power spectrum of the signal from the 220 GHz detector is biased high on all l compared to that of the signal from the 148 GHz detector.

Given the large scales of ground-based CMB experiments with thousands of telescope detectors, reducing the impact of noise on the observations of CMB temperature anisotropies and polarization is crucial to better understand the early universe, the nature of the universe, and potentially detect inflation.

Epoch of Reionization

The light from the CMB was short-lived, because as the universe expanded, the radiation redshifted to longer wavelengths; the universe became cold and dark. This era is known as the cosmic dark ages. Thus, the question arises: what caused the universe to turn the light switch on again? The CMB distributed matter evenly and smoothly across the universe, yet small density fluctuations persisted and transformed into the first protogalaxies and star-forming regions[23]. These high-density regions contracted under gravity, heating up the atoms to over 1,000 K, causing trace amounts of hydrogen molecules to form. Then, H_2 collided with hydrogen atoms, which emitted infrared radiation, cooling down the densest regions to about 200 to 300 K. Due to the low temperature and gas pressure in those regions, the clumps of gas collapsed inward and became gravitationally bound, forming the nuclear fusion cores of the first stars and galaxies in the universe[24]. These stars, categorized as Population III stars, have notable differences compared to the Sun and younger stars. Population III stars lack metal and consist of only hydrogen and helium, resulting in the inefficient production of nuclear energy at its core and thus higher surface temperatures[23].

The ultraviolet radiation produced by the first stars ionized the surrounding hydrogen. This event is known as reionization, the second phase change of hydrogen in the early universe after recombination. Bubbles of ionized gas enveloped stars, and as the bubbles grew and overlapped, ionizing radiation traveled farther in space. As more stars and galaxies formed, the universe became transparent and full of low-density, ionized hydrogen. Through nucleosynthesis and supernovae, hydrogen and helium converted to carbon, oxygen, iron, and other heavier elements[23]. The universe began to look like how it does today.

The epoch of reionization (EoR) is expected to leave a global, detectable signal, which has yet to be measured. As with the CMB, different types of noise from known and unknown sources muddle observations of the EoR, making it difficult to decipher the signal from foregrounds and noise. Many experiments are currently probing for a 21-cm signal from the EoR.

The 21 cm line

The 21-cm line, also known as the hydrogen line, is a spectral line—a stronger or weaker region in an otherwise uniform and continuous spectrum—resulting from a highly forbidden (rare)

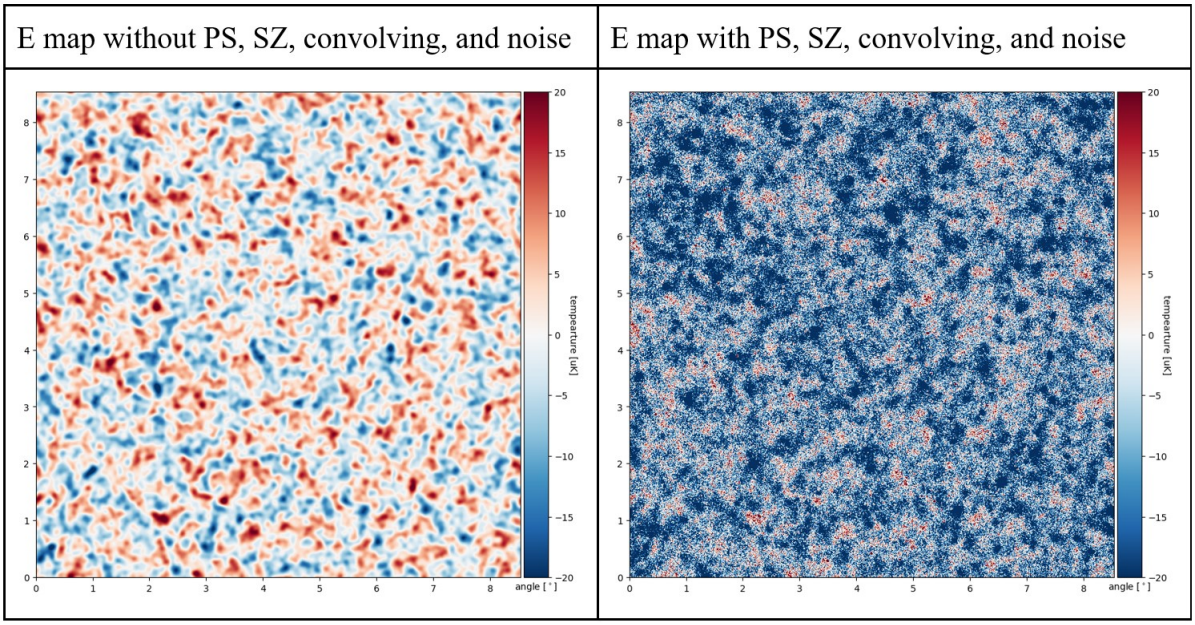

Fig. 10 (a), (b): Simulated CMB E-mode map (a) without foreground, beam convolution, and noise, i.e. the raw signal, and (b) with foreground, beam convolution, and noise.

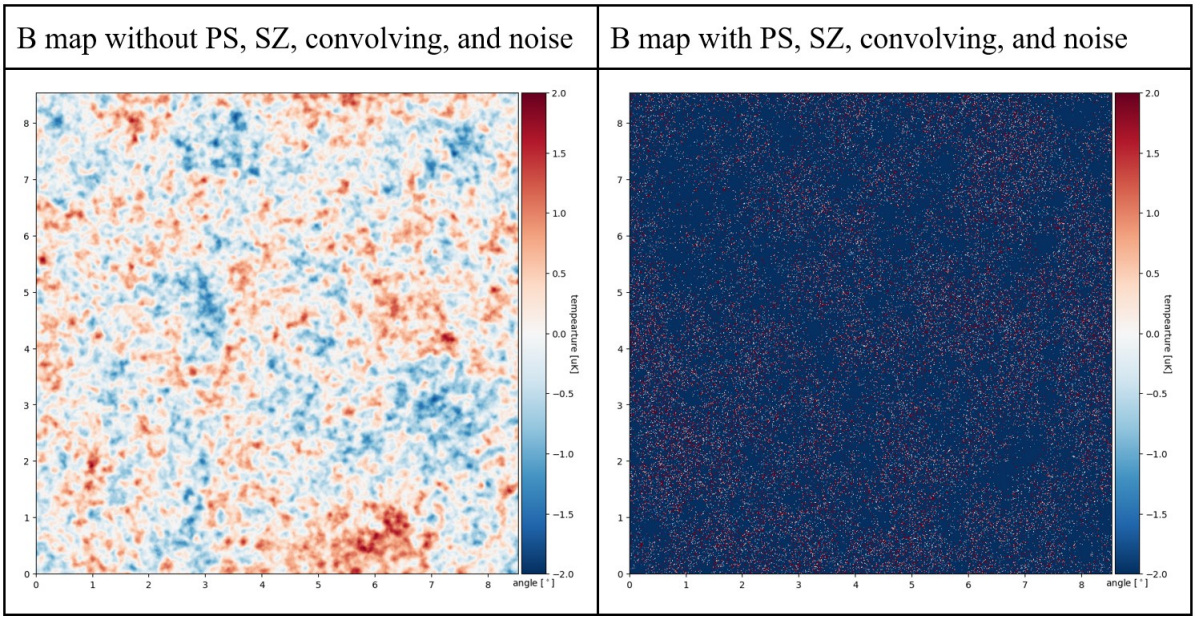

Fig. 11 (a), (b): Simulated CMB B-mode map (a) without foreground, beam convolution, and noise, i.e. the raw signal, and (b) with foreground, beam convolution, and noise.

spin-flip transition of a neutral hydrogen atom's electron[25]. After the ultraviolet energy from star formation during the epoch of reionization dissipated, free protons (ionized hydrogen atoms) and electrons formed neutral hydrogen atoms[24]. When hydrogen atoms form, the spins of the proton and electron are either anti-aligned or aligned. If the spins are anti-aligned (proton: spin-up; electron: spin-down), and the electron is at ground state, then the hydrogen atom is truly at its lowest energy state, as the electron cannot transition further to emit energy. However, if the spins are aligned (proton: spin-up; electron: spin-up), then

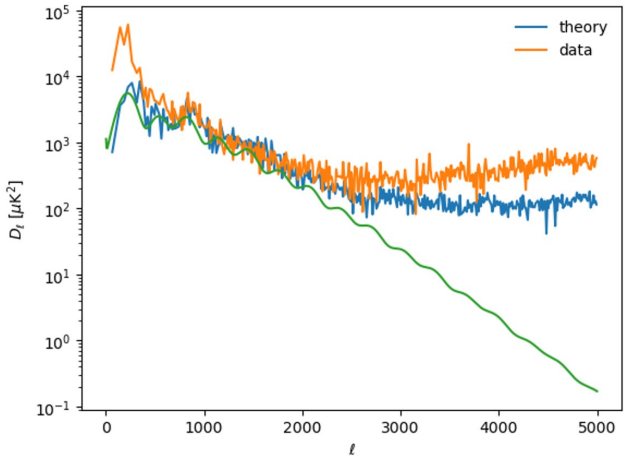

Fig. 12 The power spectra of the CMB from a simulated signal (blue), data from the ACT (orange), and the accepted power spectrum from ESA and Planck Collaboration (green).

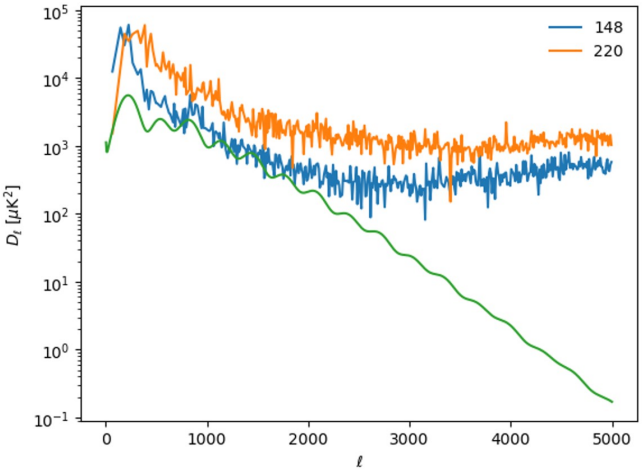

Fig. 13 The power spectra of the CMB from a 148 GHz detector in the ACT (blue), a 220 GHz detector in the ACT (orange), and the accepted power spectrum from ESA and Planck Collaboration (green).

the electron can flip its spin back down which releases energy in the form of a photon with a wavelength of 21 cm and frequency of 1420 MHz[25].

The 21-cm signal from the EoR is predicted to be observed at frequencies between about 15 MHz and 200 MHz on Earth[26]. The signal would reveal how the universe was re-ionized, as ionized hydrogen would appear as holes in the 21-cm background[27]. These holes take the form of dark patches in Figure 14, a 21-cm signal that I simulated and reproduced from tutorials by tools21cm, a Python package used by scientists in the field to analyze simulated signals of the EoR[28].

Simulating EoR signals helps to predict what the observed signal would look like and can be used to verify what is noise as

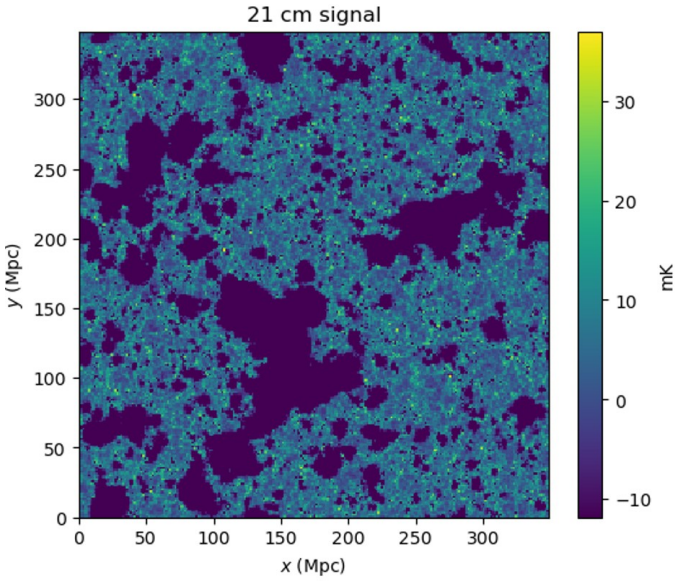

Fig. 14 Simulated 21-cm signal without foreground effects.

opposed to the actual signal. An observed EoR signal captured by a telescope would contain noise not present in the simulated signal. Land telescopes face the foregrounds of interference from television transmitters and the ionosphere. Unknown effects from other foregrounds in the galaxy may also affect the signal. The SKA-Low is a telescope located in western Australia composed of an array of antenna stations that searches for a 21-cm signal from the EoR[29]. In Figure 15, I plot the antenna configuration of the SKA-Low, reproducing the graph seen in the tools21cm tutorials[28]. This plot is helpful in adding noise to the simulated EoR signal, making it look realistic.

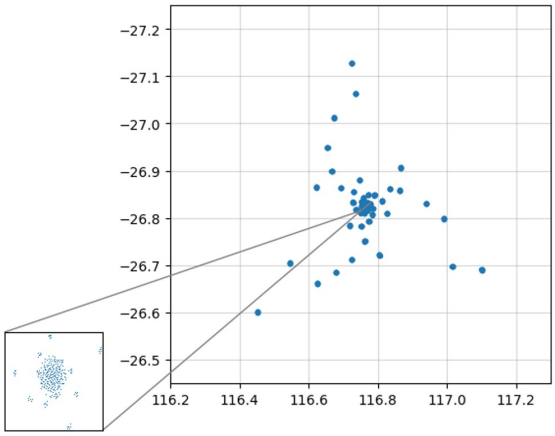

Fig. 15 Placement of SKA-Low antennae.

Most importantly, mapping the intensity of the EoR signal would provide a power spectrum that resembles Figure 15 which

I also reproduced from tools21cm[28]. Because the 21-cm line emanates from many sources rather than a single one like the CMB does, its power spectrum will reveal the environment from which the signal is emitted. The bumps on the curve correspond to a typical size of ionized bubbles surrounding stars forming during the epoch of reionization. The amplitude of the power spectrum directly relates to the neutral (average) fraction of hydrogen atoms[30].

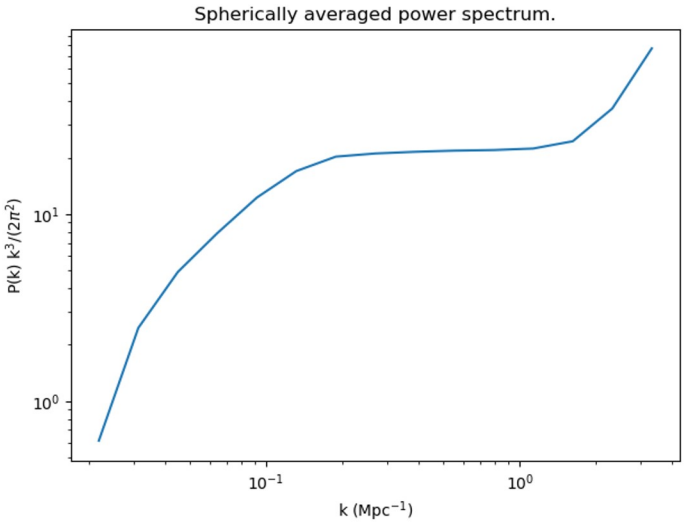

Fig. 16 Power spectrum of a simulated EoR signal. Bumps can most noticeably be seen from $k = 0.1$ to 0.2 Mpc$^-$1 and 1 and 1.1 Mpc$^-$1 where the curve is discontinuous.

Redshift-space distortions (RSDs) affect the 21-cm signal and its power spectrum as seen in Figure 16. Peculiar velocities of galaxies, i.e. when galaxies recede from Earth at speeds not proportional to their distance from Earth due to significant gravitational effect from other galaxies nearby, cause RSDs, adding a Doppler shift effect to the redshift effect from cosmological expansion[25]. On a graph, the spatial distribution of galaxies appears squashed and distorted when their positions are plotted as a function of their redshift rather than as that of their distance from the observer. Interestingly, RSDs amplify the 21-cm signal, making it easier to detect, but impede the search for non-Gaussianity, hindering intensity mapping in cosmology that helps constrain certain inflation models[31].

Besides providing information on reionization, the 21-cm line also relates to the nature of dark matter and dark energy in terms of their contributions to the accelerated expansion of the universe. Currently, dark energy is hypothesized to cause the acceleration while dark matter plays a significant role in the growth of structures in the universe and seems to interact with gravitational force but not electromagnetic force[32]. The Hydrogen Intensity and Real-time Analysis eXperiment (HIRAX), a part of the SKA-Mid configuration in South Africa, is

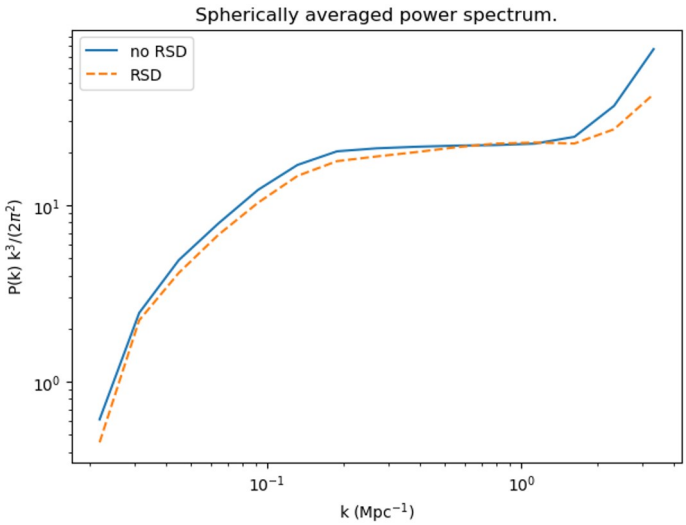

Fig. 17 The power spectra of a simulated EoR signal with no RSD (i.e. Figure 15) and with RSD.

an array of 1024 six-meter diameter radio telescopes that aims to constrain models of dark energy and dark matter using 21-cm signals. The hot neutral hydrogen emitting the 21-cm line from distant galaxy clusters and intracluster medium maps out the baryon acoustic oscillation which acts as a standard ruler for the expansion of the universe over time. If dark energy is found to be not constant, opposite to what the standard Big Bang model predicts, then the rate of acceleration of the universe may not be constant over time. The telescopes will operate between 400 and 800 MHz, which corresponds to the 21-cm line emission between redshift 0.8 and 2.5, the time period in which the standard Big Bang model predicts dark energy started affecting the universe[33].

Conclusion

This paper provides a comprehensive overview of the early stages of the universe, including advancements in their respective fields. Inflation resolves fundamental problems in the model of the universe, and detecting B modes in the CMB is currently the only means that can provide evidence for its occurrence. Noise from the environment and instruments, however, hinder the observation of the CMB, preventing current experiments to detect the B modes in CMB polarization. To analyze the effects of noise on the CMB, I simulated realistic and complete CMB temperature anisotropy signals with guidance from the CMB Analysis Summer School (2016) by Renee Hlozek and Jeff McMahon. I used Fourier transform and added foregrounds, such as point sources, SZ effect, Gaussian beam convolution, and noise maps. I analyzed the effect of different noise levels and types on the CMB signal. I also compared the angular tem-

perature power spectrum of the simulated signal to those of the observed ACT and Planck satellite signals. Ground-based telescopes seem to experience increased noise disruption when observing the CMB at higher precision, as both the power spectra of the simulated and observed ACT signals bias high compared to the accepted Planck power spectrum on larger l. Atmospheric noise, which adds strength not originally present in the CMB temperature signals, seems to be the primary factor contributing to this discrepancy, as it affects ground-based telescopes but not satellites. Moreover, ground-based telescopes with detectors of higher frequencies are more susceptible to atmospheric noise than those of lower frequencies.

While simulated signals of the early universe may not be completely accurate, they provide valuable insight into visualizing what an undetected phase of the universe may look like with or without noise and can later be used to verify the observed signal. The next steps in this research would be to improve the detectors and telescopes currently observing the CMB and probing its polarization for inflationary gravitational waves. Furthermore, as the EoR has yet to be detected, a similar study can be performed, simulating the signal with various types of noise and later comparing the simulated signal to the observed one.

References

1 L. Gurevich, *Astrophysics and Space Science*, **38**, 67–78.

2 A. Guth, *Physical Review D*, **23**, 347–356.

3 A. Guth and S. Tye, *Physical Review Letter*, **44**, 631–635.

4 A. Lightman, *Ancient Light: Our Changing View of the Universe*, Harvard University Press.

5 J. Peacock, *Cosmological Physics*, Cambridge University Press, Cambridge.

6 M. Bastero-Gil, A. Berera, R. Ramos and J. Rosa, *Physics Letters B*, **813**, 1–6.

7 S. Odintsov, V. Oikonomou, I. Giannakoudi, F. Fronimos and E. Lymperiadou, *Symmetry*, **15**, 1–69.

8 R. Dicke, P. Peebles, P. Roll and D. Wilkinson, *The Astrophysical Journal*, **142**, 414–419.

9 B. Abbott, *Microwave (WMAP) All-Sky Survey*, `http://www.haydenplanetarium.org/universe/duguide/exgg_wmap.php`.

10 M. Turner, *Scientific American*, **301**, 36–43.

11 A. Penzias and R. Wilson, *The Astrophysical Journal*, **142**, 419–421.

12 D. Fixsen, *The Astrophysical Journal*, **707**, 916–920.

13 D. Fixsen, E. Cheng, J. Gales, J. Mather, R. Shafer and E. Wright, *The Astrophysical Journal*, **473**, 576–587.

14 R. Sachs and A. Wolfe, *The Astrophysical Journal*, **147**, 73–90.

15 P. Valageas, A. Balbi and J. Silk, *Astronomy Astrophysics*, **367**, 1–17.

16 P. Ade, *Astronomy and Astrophysics Journal*, **571**, 1–60.

17 A. Lewis and S. Bridle, *Physical Review D*, **66**, 103511.

18 K. Abazajian, *CMB-S4 Science Book*.

19 M. Kamionkowski and E. Kovetz, *Annual Review of Astronomy and Astrophysics*, **54**, 227–269.

20 A. Lewis and A. A. Lasenby, *The Astrophysical Journal*, **538**, 473–476.

21 D. Samtleben, S. Staggs and B. Winstein, *Annual Review of Nuclear and Particle Science*, **57**, 245–283.

22 J. Sievers, *Journal of Cosmology and Astroparticle Physics*, 1–26.

23 R. Larson and V. Bromm, *Scientific American*, **12**, 4–11.

24 V. Bromm, N. Yoshida, L. Hernquist and C. McKee, *Nature*, **459**, 49–54.

25 J. Pritchard and A. Loeb, *Reports on Progress in Physics*, **75**, 1–64.

26 W. Peters, T. Lazio, T. Clarke, W. Erickson and N. Kassim, *Astronomy Astrophysics*, **525**, 1–7.

27 K. Kohler, N. Gnedin, J. Miralda-Escude and P. Shaver, *The Astrophysical Journal*, **633**, 532–559.

28 S. Giri, G. Mellema and H. Jensen, *The Journal of Open Source Software*, **5**, 2363.

29 E. Lera Acedo, N. Razavi-Ghods, N. Troop, N. Drought and A. Faulkner, *Experimental Astronomy*, **39**, 567–594.

30 H. Shimabukuro, K. Hasegawa, A. Kuchinomachi, H. Yajima and S. Yoshiura, *Publications of the Astronomical Society of Japan*, **75**, 1–32.

31 S. Bharadwaj, A. Mazumdar and D. Sarkar, *Monthly Notices of the Royal Astronomical Society*, **493**, 594–602.

32 M. Turner, *Physica Scripta*, 1–22.

33 D. Crichton, *Journal of Astronomical Telescopes, Instruments, and Systems*, **8**, 1–24.